Free vibration analysis of locally damaged aerospace tapered composite structures using component-wise models

Free vibration analysis of locally damaged aerospace tapered composite structures using component-wise models

A. Viglietti[a], E. Zappino[a,b], E. Carrera[a]

[a]MUL^2 Group, Department of Mechanical and Aerospace Engineering, Politecnico di Torino
[b]Corresponding Author, email: enrico.zappino@polito.it

Abstract

This work presents the free vibration analysis of tapered aircraft structures made of composite and metallic materials, with reference to global and local damage. A refined one-dimensional model, developed in the framework of the Carrera Unified Formulation, has been used to provide a detailed description of structures. Multi-component aeronautical structures have been modeled adopting Lagrange polynomials to evaluate the displacement field over the cross-section. Each component has been described through the component-wise approach, with its own geometrical and mechanical characteristics. The effects of localized damage have been investigated, thanks to the accuracy of the layer-wise models adopted. The model has been assessed by comparing the results with classical FE models. The results show that the present approach provides an accurate solution for the free vibration analyses of complex structures and is able to predict the consequences of a global or local failure of a structural component. The computational efficiency and the accuracy of the model used in this work can be exploited to characterize the dynamic response of complex composite structures considering a large number of damage configurations.
Keywords: CUF, One-dimensional model, tapered beam, Composite material, Failure

---

1. Introduction

Aeronautical structures are composed of several components that distribute the loads they undergo. An increasing number of aeronautical parts are made of composite materials for weight saving purposes. It is clear that, given the multi-component nature of these kinds of structures, if one component fails, the stress distribution and the structural behavior changes according to the entity of the damage. The knowledge of these effects is a crucial point in the design process to increase the structural reliability and the safety factor. Moreover the timely damage detection of damage is important for maintenance programs. Several nondestructive tests, such as ultrasounds or the magnetic field test, already exist. However, an estimation of the location of the damage is required to increase the efficiency of these methods. The presence of the damage affects the dynamic response of a structure, and the variations in the frequencies and modal shapes can be used to detect structural damage. Several works on this kind of damage detection have been proposed. Zhang *et al.*[1] and Capozzucca [2] proposed analyses of damaged composite beams, studying vibration behavior. The work of Wang [3] used an FE method to detect damage in wind turbine blades considering variations of the modal shape curvatures. Nguyen [4] proposed a study on the detection of damage in which calculating the modal shapes were calculated using three-dimensional beam elements. Pollayi and Yu [5] investigated the mechanical behavior of a damaged rotor and wind turbines using beams, on the basis of the geometrically nonlinear 3-D elasticity theory and the variational asymptotic beam sectional analysis (VABS). Pérez et al. [6] adopted a different approach and performed extensive experimental analyses on the vibration of damaged laminates. The presence of damage and the characteristics of the damage can be estimated by referring to a database that includes information on the natural frequencies and model shapes of a wide spectrum of damaged cases, using accurate measurements of the real structure. This database can only be achieved through mathematical model analyses because a great deal of experimental proofs is not recommended because of time and money constraints. These models should be able to provide very accurate displacement and strain/stress fields. Damage introduces local and non-classical effects, which cannot always be detected by the conventional FE models that are used in the aeronautic field. A three-dimensional analysis is required to provide accurate results, but this can lead to huge computational costs. In this work, an advanced beam model based on the Carrera Unified Formulation is proposed to deal with damaged structures in order to obtain accurate results, but with low computational costs expressed in terms of Degrees of Freedom (DOFs). Classical theories, such as the Euler-Bernoulli beam model [7] or the Timoshenko beam model [8], are not suitable for damage detection. In the last few years, many works have been proposed to extend the application of one-dimensional models to any geometry, boundary condition or, mechanical complexity. In the aeronautical field, for aerodynamic reasons, particular shapes such as tapered shape or twist angle, are used. These factors increase the structural complexity and, as a result, more complex models are required. Tapered shapes are considered in this work. In this way, if the beam axis is placed in the y-axis direction, the bending stiffness $EI(y)$ changes along the axis. The classical approximation introduced to deal with such geometries is a step-by-step approach, which involves the subdivision of the structure into several rigidly prismatic beams with different cross-sections. The approximation is improved by increasing the number of subdivisions. Analytical methods,

[8][9] are used to introduce the shear stress of a tapered beam. After the introduction of the FE method, several works have been proposed. A modified stiffness matrix for tapered components has been proposed by Just [10]. This work uses modified displacement functions which consider the variations in the proprieties of the sections. Brown [11] presented a stiffness matrix formulation for a linearly tapered beam, while Schreyer [12] proposed a beam theory for tapered beams, in which the shear strain is considered Many works have been proposed about aeronautical structures in the framework of the Carrera Unified Formulation. In the present 1-D CUF model, the displacement field over the cross-section is described through expansion functions. This feature allows the model to deal with arbitrary geometries, materials, and boundary conditions. After the first models, which were based on Taylor expansions, Lagrange polynomials were introduced. In this way, multi-component structures can be modeled through *ad-hoc* formulations of each component (Component-Wise approach) [13]. Some of the works about this approach and its capability in the aerospace field are those of [14][15] and [16]. The work of [17] deals, through the CW approach, with different prismatic structures made of an isotropic material; several several types of damage were considered. The frequencies were evaluated for each case and the modal shapes were compared using MAC (Modal Assurance Criterion)[18]. This criterion has already been employed in the civil field (damaged bridges) by Salawu and Williams [19]. The extension of the models to tapered structures has been proposed in [20] and [21].

In this work some aircraft structures with a tapered shape are analyzed using a 1-D CUF model, considering different types of damage. The paper is organized as follows. A first part concerns the one-dimensional model: the theory, finite element solution and model of the damage are presented. Subsequently, several results are discussed and, finally, the main remarks are presented.

2. Refined one-dimensional models formulation

The damage detection through free vibration analyses requires models with three-dimensional capabilities able able to deal with complex local phenomena. Here, the Carrera Unified Formulation is presented to develop a one-dimensional refined model able to deal with this topic. After some preliminaries, the basis and the advantages of the CUF are presented in this section, finally, the damage modeling approach is introduced.

Preliminaries

At first, it's necessary to define the work space of this formulation. Two frames are used to achieve the model of a structure. The first frame (x_G, y_G, z_G) is the global coordinate system of the three-dimensional space. The beams formulation is derived at the local level, respect a second frame (x, y, z). y is the local beam axis and x, z represent the plane of the beam cross-section. The beam model derived at the local level can be arbitrary placed in the space using rotations and translations. These frames are shown in Figure 1a.

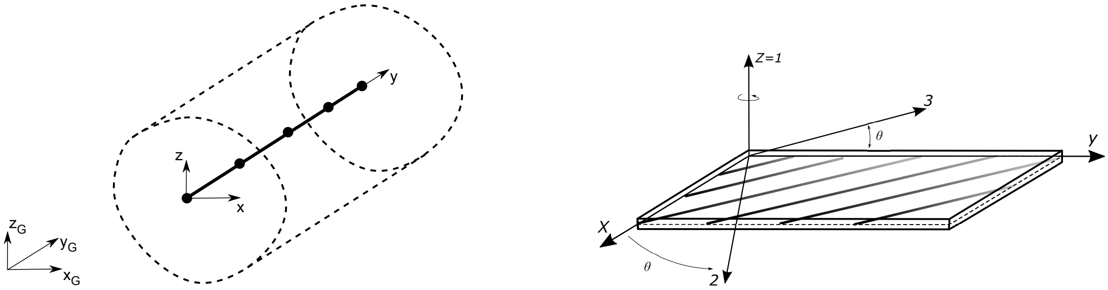

(a) Beam Coordinate frames. (b) Material Coordinate frames.

Figure 1: Reference frames.

The reference system $(1, 2, 3)$ is the material reference system. The local displacement vector is expressed as:

$$\boldsymbol{u}^T(x, y, z) = \{u_x \, u_y \, u_z\} \tag{1}$$

The stress vector $\boldsymbol{\sigma}$ and the strain one $\boldsymbol{\epsilon}$ are achieved as:

$$\boldsymbol{\sigma}^T(x, y, z) = \{\sigma_{xx}, \sigma_{yy}, \sigma_{zz}, \tau_{xy}, \tau_{xz}, \tau_{yz}\} \tag{2}$$

$$\boldsymbol{\epsilon}^T(x, y, z) = \{\epsilon_{xx}, \epsilon_{yy}, \epsilon_{zz}, \epsilon_{xy}, \epsilon_{xz}, \epsilon_{yz}\} \tag{3}$$

The strain vector is defined with the following linear strain-displacement relation:

$$\boldsymbol{\epsilon} = \boldsymbol{b}\boldsymbol{u} \tag{4}$$

where $\boldsymbol{b}$ is a differential operator (a 6×3 matrix). The components of this matrix can be found in the book by Carrera *et al.* [22].

Hook's law provides the stress vector defined with the following equation:

$$\boldsymbol{\sigma} = \boldsymbol{C}\boldsymbol{\epsilon} \tag{5}$$

where $\boldsymbol{C}$ is the 6×6 material coefficient matrix. It's a symmetric matrix, then $C_{ij} = C_{ji}$. $\boldsymbol{C}$ changes the components respect the kind of considered material. A *anisotropic* material which has a different behavior in any direction, is composed of 21 independent coefficients. Instead, if the proprieties are the same along three perpendicular planes, the material is defined as *orthotropic* material and the coefficients become nine components. In this case, the matrix $\boldsymbol{C}$ is defined as:

$$\boldsymbol{C} = \begin{bmatrix} C_{11} & C_{12} & C_{13} & 0 & 0 & 0 \\ C_{21} & C_{22} & C_{23} & 0 & 0 & 0 \\ C_{31} & C_{32} & C_{33} & 0 & 0 & 0 \\ 0 & 0 & 0 & C_{44} & 0 & 0 \\ 0 & 0 & 0 & 0 & C_{55} & 0 \\ 0 & 0 & 0 & 0 & 0 & C_{66} \end{bmatrix} \tag{6}$$

The matrix are composed by 12 terms, but due to the symmetry of the matrix, $C_{12} = C_{21}$, $C_{13} = C_{31}$ and $C_{23} = C_{32}$. For this reason the matrix is reduced to 9 components. With this type of material, the preferential direction of the material should be defined. For this reason, a third reference system is introduced referred to the material. This frame is figured in 1b. An example of an orthotropic material is a fiber-reinforced layer. This layer lies on the plane 23 which is parallel to the plane xy. The axis 1 is aligned with the z-axis. Considering the axis 3 as the fiber direction, this one can be rotated with an angle of θ respect the y-axis. A positive counterclockwise rotation is considered. The present formulation allows the material to be oriented in an arbitrary direction to achieve particular lamination. As a consequence the transformation matrix $\boldsymbol{T}$ is introduced:

$$\boldsymbol{C} = \begin{bmatrix} cos^2\theta & sin^2\theta & 0 & 0 & 0 & sin2\theta \\ sin^2\theta & cos^2\theta & 0 & 0 & 0 & -sin2\theta \\ 0 & 0 & 1 & 0 & 0 & 0 \\ 0 & 0 & 0 & cos\theta & -sin\theta & 0 \\ 0 & 0 & 0 & sin\theta & cos\theta & 0 \\ -cos\theta sin\theta & cos\theta sin\theta & 0 & 0 & 0 & cos^2\theta - sin^2\theta \end{bmatrix} \tag{7}$$

A *transformed material stiffness matrix* is introduced and it is expressed with the following form

$$\tilde{\boldsymbol{C}} = \boldsymbol{T}\boldsymbol{C}\boldsymbol{T}^{\boldsymbol{T}} \tag{8}$$

This is the new stiffness matrix to be introduced in the Hooke's law.

$$\boldsymbol{\sigma} = \tilde{\boldsymbol{C}}\boldsymbol{\epsilon} \tag{9}$$

If the material has the same behavior in all directions, it is a *isotropic* material. Over any direction, the material provides the same behavior. In this case, there is no need to define a material reference system and a rotation matrix. The performance of the material can be described with only one value of the Poisson ratio and of Young's modulus. These assumptions lead to have

$$C_{11} = C_{22} = C_{33} \qquad C_{12} = C_{13} = C_{23} \qquad C_{44} = C_{55} = C_{66} \tag{10}$$

The explicit forms of $\boldsymbol{C}$ terms can be found in the books by Tsai [23] or Reddy [24].

Cross-sectional approximation

The 1-D Carrera Unified Formulation (CUF) introduces the displacement field $\boldsymbol{u}$ as the product of two contributions, one over the cross-section and one along the beam axis:

$$\mathbf{u}(x, y, z) = F_\tau(x, z)\mathbf{u}_\tau(y), \qquad \tau = 1, 2 \dots M, \tag{11}$$

where $\mathbf{u}_\tau$ is the displacement vector, F_τ represents an expansion used to approximate the behavior of the beam cross-section and M is the number of the expansion terms. Depending on the used expansion, different classes of CUF model have been developed in the year, and two main classes have emerged. A first class uses the Taylor expansion as $F_\tau(x, z)$. Considering the TE model (TE: Taylor expansion) of the first order, the displacement field of the term u_x, for example, is expressed as follow:

$$u_x = u_{x_1} + x u_{x_2} + z u_{x_3} \tag{12}$$

The TE models can be deepened in [25]. The second class of CUF model uses the Lagrange polynomials to describe the cross-section through high-order elements. These model, using an isoparametric formulation, allow us to built different multi-node elements in the natural domains. In this way, the model can describe the cross-section geometry without introducing approximations in the real domain. The model used in this paper employs this expansion. Several sets of Lagrange polynomial exist, but in this work, in order to improve the accuracy, the nine-point set (L9) have been adopted. Other sets are for example L4 elements or L3 elements. More detail can be found in [26]. These functions, introducing as unknowns only translational displacements, have the following forms:

$$
\begin{aligned}
&F_\tau = \frac{1}{4}(r^2 + r * r_\tau)(s^2 + ss^\tau) \qquad \tau = 1,3,5,7 \\
&F_\tau = \frac{1}{2}s^2{}_\tau(s^2 + ss_\tau)(1 - r^2) + \frac{1}{2}r^2{}_\tau((r^2 - rr_\tau)(1 - s^2) \qquad \tau = 2,4,6,8 \\
&F_\tau = (1 - r^2)(1 - s^2) \qquad \tau = 9
\end{aligned}
\tag{13}
$$

where r and s can be a value beetween -1 an $+1$ and r_τ and s_τ are the coordinates of the nine points in the natural coordinate frame. In this way, considering the L9 element, the formulation of the displacement becomes:

$$
\begin{aligned}
u_x &= F_1 u_{x_1} + F_2 u_{x_2} + F_3 u_{x_3} \ldots + F_9 u_{x_9} \\
u_y &= F_1 u_{y_1} + F_2 u_{y_2} + F_3 u_{y_3} \ldots + F_9 u_{y_9} \\
u_z &= F_1 u_{z_1} + F_2 u_{z_2} + F_3 u_{z_3} \ldots + F_9 u_{z_9}
\end{aligned}
\tag{14}
$$

where $u_{x_{b1}} \ldots u_{x_{b9}}$ represent the components x of the displacement field of each node of the L9 element.

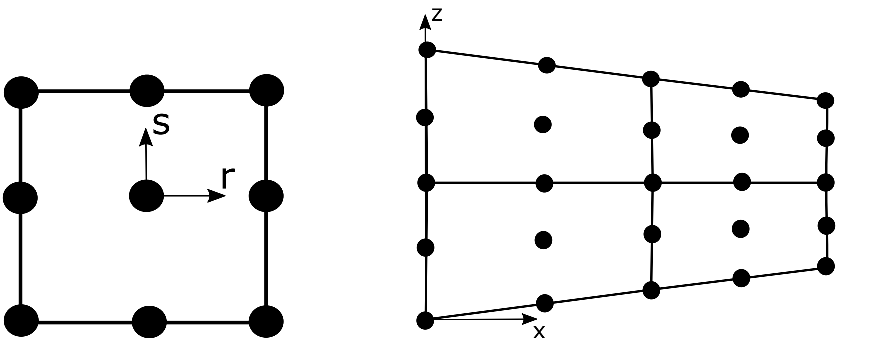

(a) L9 element in the natural coordinate system.

(b) Four assembled L9 elements in the beam reference frame.

Figure 2: L9 elements.

Figure 2 shows on the left the L9 element in the natural reference system. Carrera and Petrolo [27] has demonstrated as the accuracy can be increased by using several L-elements in order to have a better refinement of the cross-section. The L-elements can be assembled as indicated on the right of figure 2.

Finite Element formulation

In order to solve the one-dimensional problem, the Finite Element model is used. The shape functions N_i are introduced to approximate the displacement over the beam axis (y) and then the vector $\boldsymbol{u}$ can be written as

$$\mathbf{u}(x, y, z) = F_\tau(x, z) N_i(y) \mathbf{q}_{\tau i} \tag{15}$$

where $\mathbf{q}_{\tau i}$ is the nodal displacements vector.

The B3 elements (elements with three nodes) are adopted in this work and the index i indicates the node of the beam element. The shape functions can be arbitrarily chosen; the shape functions used in this work are reported in [22].

The governing equations can be obtained using the PVD (Principle of Virtual Displacements). The term δ denotes the virtual variation.

$$\delta L_{int} = -\delta L_{ine} \tag{16}$$

The two members of 16 are respectively the variation of the strain energy and the variation of the work performed by the inertial loads. The internal work can be written as follow:

$$\delta L_{int} = \int_V \delta \boldsymbol{\epsilon}^T \boldsymbol{\sigma} dV \tag{17}$$

The terms showed in 17 are already known. Expanding the inertial work the following form is obtained:

$$\delta L_{ine} = \int_V \delta \boldsymbol{u}^T \rho \ddot{\mathbf{u}} dV \tag{18}$$

where ρ is the density of the material and $\ddot{\mathbf{u}}$ is the acceleration vector.

From 17 and 18 the stiffness matrix $\boldsymbol{K}$ and the mass matrix $\boldsymbol{M}$ are achieved in terms of *fundamental nucleus* (FN), a 3x3 block with fixed form. Its components are reported in [17]. A complete description of the FN derivation and its use to achieve the global matrices are presented in [22].

For the sake of clarity, the form of the stiffness FN is now presented. Introducing the Hooke's law and the geometrical relations, the internal work can be expressed in function of the shape functions, the expansion used for the cross-section and the properties of the material.

$$\delta L_{int} = \delta \mathbf{q}_{sj}^T \int_V N_j(y) F_s(x,z) \mathbf{b}^T \mathbf{C} \mathbf{b} F_\tau(x,z) N_i(y) dV \, \mathbf{q}_{\tau i} \tag{19}$$

The integral is the stiffness FN $\mathbf{k}^{ij\tau s}$ Each term of the fundamental nucleus has a fixed form. Equation 20 shows the extended formulation of two terms of the fundamental nucleus. The other terms can be obtained by the permutation of the indexes. The global stiffness matrix can be achieved varying the indexes i,j,τ and s.

$$\begin{aligned} k_{xx}^{\tau sij} =& (\lambda + 2G) \int_l N_i N_j dy \int_A F_{\tau,x} F_{s,x} dA + G \int_l N_i N_j dy \int_A F_{\tau,z} F_{s,z} dA \\ &+ G \int_l N_{i,y} N_{j,y} dy \int_A F_\tau F_s dA; \\ k_{xy}^{\tau sij} =& \lambda \int_l N_{i,y} N_{j,y} dy \int_A F_\tau F_{s,x} dA + G \int_l N_i N_j dy \int_A F_{\tau,x} F_s dA; \end{aligned} \tag{20}$$

Each beam can be arbitrary oriented in the space, the rotations and translation can be applied at each fundamental nucleus, as shown in [28], in order to write the global matrices in the global reference system. In this way, by imposing the congruence of the displacements in some nodes defined by the geometry, a complex structure can be obtained. More details can be found in [28] where the assembly procedure has been also described.

Knowing the form of $\boldsymbol{K}$ and $\boldsymbol{M}$, the 16 can be rewritten as follows:

$$\boldsymbol{M}\ddot{\boldsymbol{u}} + \boldsymbol{K}\boldsymbol{u} = 0 \tag{21}$$

This is the undamped dynamic problem. Considering harmonic solutions and using the classical eigenvalue problem, the natural frequencies ω_k can be obtained.

$$(-{\omega_k}^2 \boldsymbol{M} + \boldsymbol{K}) \boldsymbol{u_k} = 0 \tag{22}$$

where $\boldsymbol{u_k}$ is the kth eigenvector.

Damage model description

In this work the damage has been introduced through a degradation of the material properties in a localized area. The following formulation has been used:

$$E_d = d \times E, \qquad with \qquad 0 \leq d \leq 1 \tag{23}$$

where E is Young's modulus of the undamaged material. E_d is the modulus of the deteriorated material while d is the damage level. For $d = 1$ the material is undamaged while for $d = 0$ the material is completely damaged, intermediate values can be used. Considering an orthotropic material, the terms $E_{22}, E_{33}, G_{12}, etc$, are degraded in the same way. Thanks to the capabilities of the present model, the damage can be introduced in the problem at different levels, as shown in Figure 3. Considering a tapered panel with two stringers the damage can be introduced at the component level, as in the case of a damaged stringer. Otherwise the damage can be introduced at the layer level, as in the case in which just one layer collapses or, eventually, the damage can be reduced only in a local area. In this case the degradation of the material has been included locally. This approach can reproduce the situation in which just a small part of the structure is damaged as in the case of local impacts. These concepts are more clear through the picture 3 which represents the damage.

3. Numerical Results

The following results refer to all the damage situations that can be investigated using the present model: a component failure, a layer failure and local damage. Moreover, a complex structure has been investigated to demonstrate the capabilities of the present approach in the analysis of real configurations.

3.1. Three stringer reinforced panel

The reinforced structure shown in Figure $4a$ is considered. There are two panels with different tapered shapes, which are reinforced by three square cross-section stringers. The panels are made of a composite laminate, which has 4 layers lamination of $0°/90°/90°/0°$. The longitudinal axis of the material, in the case of $\theta = 0°$, coincides with the y_G axis. The composite material is a *CFRP: Carbon Fiber Reinforced Polymer* with the following proprieties: $E_{LL} = 50\ GPa$, $E_{TT} = E_{ZZ} = 10\ GPa$, $G = 5\ GPa$, Poissons's ratio $\nu = 0.25$ and density of 1700 kg/m^3. E_{LL} refers to the fiber direction. The reinforcements are made of an aluminum alloy. The Young

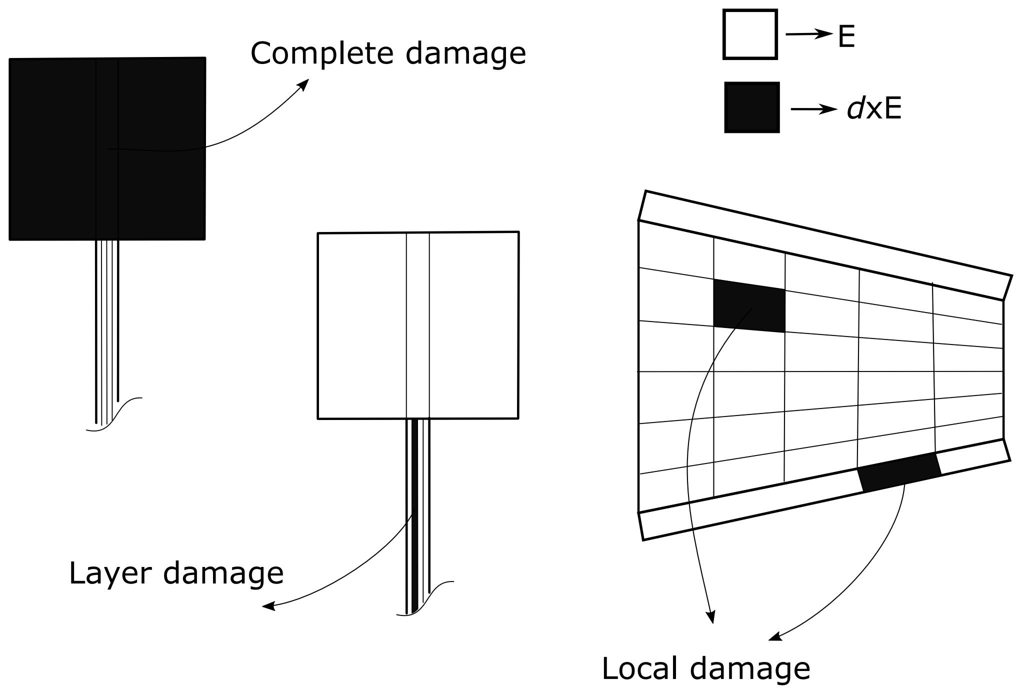

Figure 3: Different damage configurations: at a component level (stringer), at a layer level and at a local level.

Modulus is equal to $E = 71.7\ GPa$ and ν is equal to 0.3. The alloy has a density of 2810 kg/m^3. The dimensions of the structures are: $L = 2$, $h_1 = 0.48$, $h_2 = 0.98$, $h_3 = 0.2$ and $h_4 = 0.4$. All the dimensions are expressed in meters. The stringers have a square cross-section with an area equal to 0.0016 m^2. The central stiffener is parallel to the y_G axis.

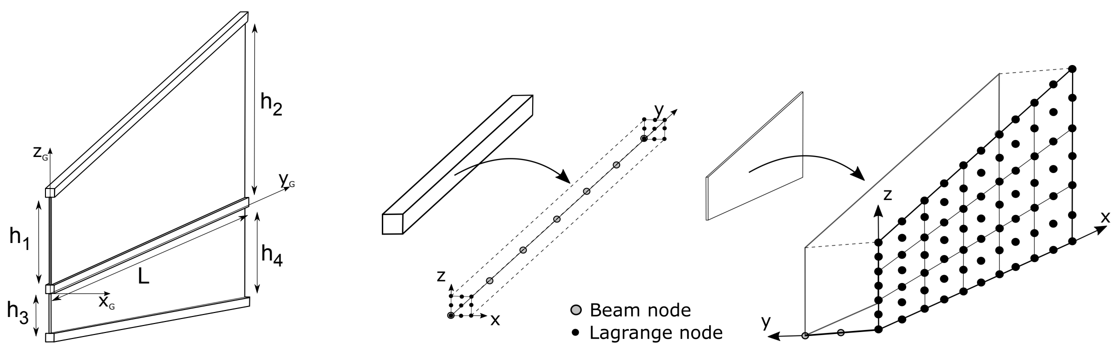

(a) 3-stringer panel

(b) FEM description

Figure 4: Three stringer reinforced panel: model description.

The reinforcements are described with six 4-node beam elements placed along the length of the component, and the square cross-section is described with three L9 elements.

The panel is described using 3-node beam elements over the thickness of each layer. The tapered shape of the panel (the cross-section of the local beam) is made up of L9 elements (9×5 for the top panel and 9×4 for the bottom one). Figure 4*b* shows the details of the model. The panel is represented by a cross-sectional mesh of 5×3 L9 elements. More details about this approach used to describe composite panels can be found in [20] and [21].

3.2. Undamaged Panel

The undamaged panel has been investigated to assess of the model. The results have been compared with those obtained using different models built using the commercial Nastran code. The first model is a solid one (3D), while the second one uses shell elements for the panels and beams for the stringers (1D-2D). Table 1 shows the first 15 frequencies obtained for the different models. The first six columns report the classical theories and TE CUF Models. A step-modeling approach was used for these models to approximate the tapered shape. Twenty beam elements were adopted to discretize the structure. The solid model, which can can be considered as the reference model, was built using HEX8 solid elements. This approach leads to the very high number of degrees of freedom, even when only one element is used through the thickness of each lamina The component-wise model which is based on a Lagrange polynomial expansion (the LE Model) is reported in the eighth column.

Classical theories are only able to identify the first frequency that is the first bending mode. TE 3^{ed} and 4^{th} order models can detect the first two bending modes, but they fail to consider shell-like behavior. The LE model model provides comparable frequencies with those of the 3D Nastran model. Figure 6*a* presents a comparison of the modal shapes for the present LE model and the solid model. The MAC (Modal Assurance Criterion) was used to correlate the modal shapes that ware obtained using different models. MAC values equal to 1 mean that the two analyzed modal shapes correspond. The picture shows that the current LE model is able to detect all of the first 15 modes whit a good correlation value if compared with the modes obtained using the solid model.

The Nastran 1D-2D model was also considered since this modeling approach is widely used in the aeronautical field. Sensible errors emerged, with respect to the the reference 3D values. The related MAC graph shows the difficulty this model has in detecting the modal shapes at higher frequencies. These differences are due to the approximations introduced to the connections between the stringer and the panel. This phenomenon was discussed in detail in the work by Cavallo *et al.*[29]. Figure 5 shows the first ten modal shapes of the studied structure.

	EBBT	TBT	Taylor step-wise models N=1	N=2	N=3	N=4	LE model	Nastran Models 1D-2D	3D
DOF's	63	105	189	379	630	945	13167	38300	179700
f_1	8,63	8,63	8,63	7,83	7,61	7,52	7,14	7,08	7,14
f_2	53,46	53,46	53,46	30,42	29,09	28,11	7,89	7,83	7,96
f_3	150,29	150,29	150,29	48,57	47,18	46,49	12,31	11,51	13,58
f_4	274,84	274,84	274,78	98,01	91,47	86,20	13,02	12,58	14,53
f_5	298,15	298,15	298,15	136,84	132,82	127,89	18,02	16,57	20,49
f_6	501,70	501,70	490,30	204,73	185,90	135,12	23,75	21,67	26,62
f_7	679,45	679,45	501,70	254,51	188,72	175,55	28,44	25,7	30,26
f_8	766,74	766,74	603,79	271,89	241,32	202,38	32,54	26,98	32,99
f_9	785,99	785,99	785,26	361,31	262,50	233,22	36,07	31,67	38,43
f_{10}	1100,92	1100,92	766,73	458,16	296,29	257,21	41,33	34,7	42,35
f_{11}	1496,35	1496,35	1100,89	575,28	328,73	307,68	46,97	41,06	46,73
f_{12}	1513,93	1513,93	1181,44	588,61	426,39	370,59	47,57	43,28	47,80
f_{13}	1713,54	1713,54	1494,67	602,32	447,16	425,21	49,62	45,28	50,10
f_{14}	2017,58	2017,58	1513,87	702,43	522,09	490,40	50,85	46,43	50,85
f_{15}	2018,81	2018,81	1736,34	727,94	585,97	541,10	52,98	48,92	54,18

Table 1: First 15 frequencies of the 3-stringer composite panel obtained using different models.

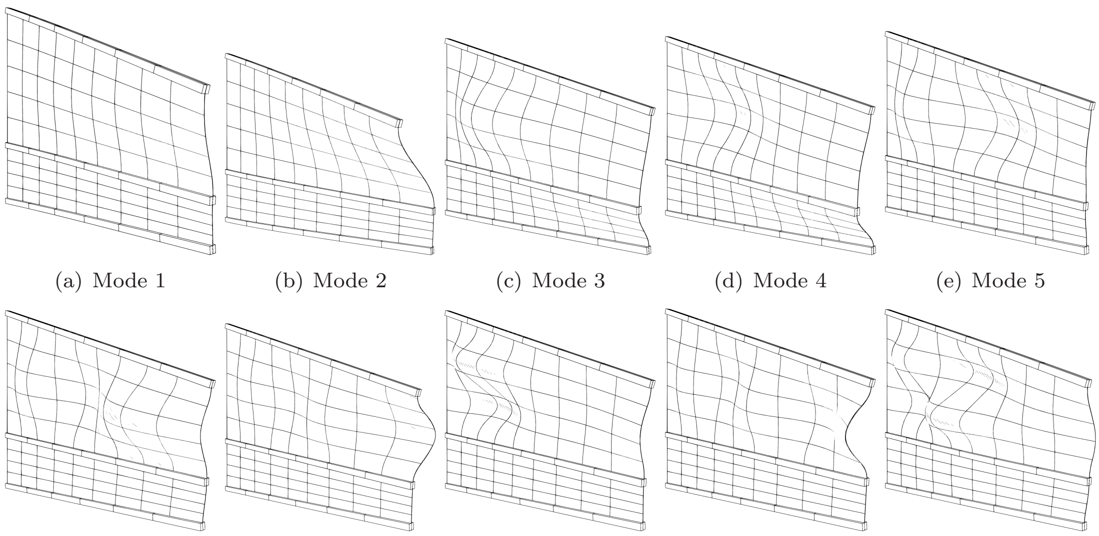

(a) Mode 1 (b) Mode 2 (c) Mode 3 (d) Mode 4 (e) Mode 5

(f) Mode 6 (g) Mode 7 (h) Mode 8 (i) Mode 9 (j) Mode 10

Figure 5: First 10 modal shapes evaluated using the LE model.

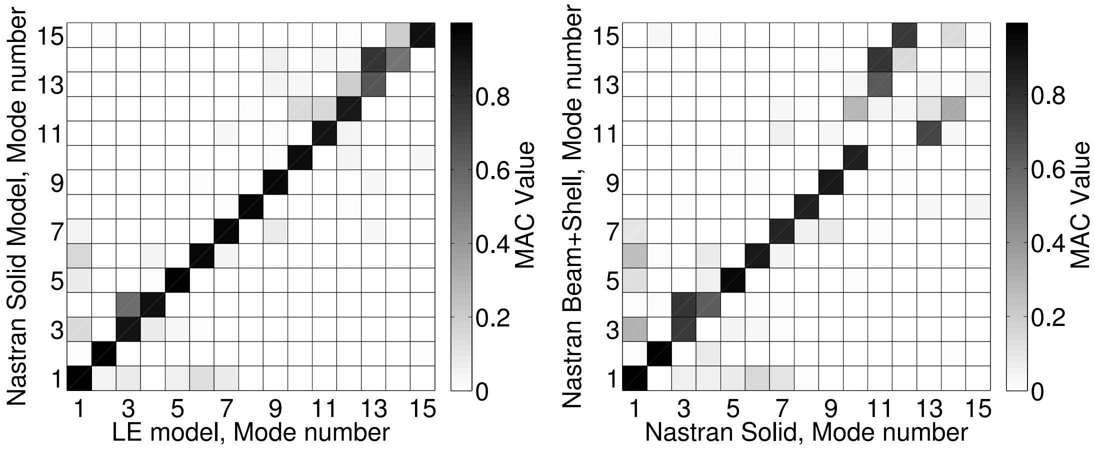

(a) LE model VS 3D Model

(b) 3D Model VS 1D-2D Model

Figure 6: Correlation of the modal shapes of the undamaged structure evaluated using different models.

In conclusion the present assessment shows that the here adopted LE model is able to provide a comparable accuracy with that of solid models, with a marked reduction in the computational costs. Therefore, the present LE model has been used in the following sections to investigate damaged structures.

3.3. Damaged Panel

In this section, several types of damage have been considered. The first part concerns a component that is completeld damaged. First the upper reinforcement was considered damaged. The free-vibration characteristics were evaluated and compared with those of the undamaged case. Then, the same process was applied to the top panel, the central stiffener and the bottom panel,one by one. These damage cases are presented in Figure 7. In the second part, the damage was considered at the layer level. An external and an internal layer were considered damaged in order to evaluate the worst case. Local damage was therefore introduced and the effects due to its position were investigated. Three different levels of degradation, d, were considered for each damage case: $d = 0.9$, $d = 0.5$ and $d = 0.1$. In the last case, the damaged components only had the 10% of the original stiffness.

3.3.1. Stiffened panel with a damaged component

In this section, the damage has been considered at the component level. Figure 7 shows the four considered cases.

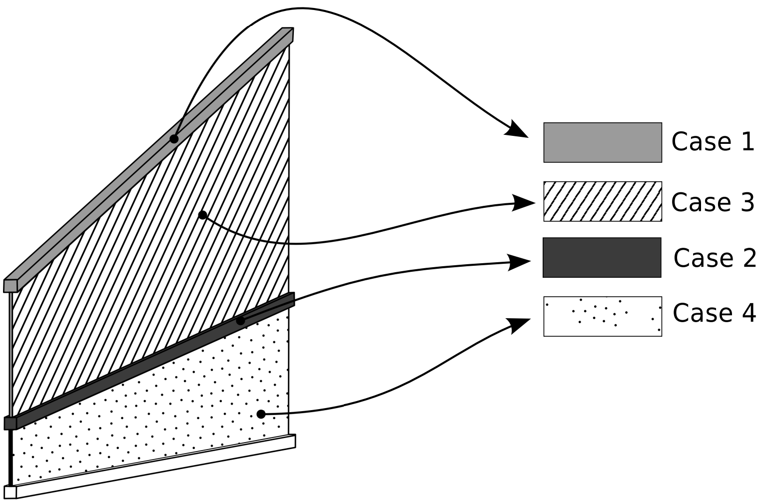

Figure 7: Damage at the component level: The considered cases.

	Undamaged	Case 1			Case 2			Case 3			Case 4		
	d=0	d=0.9	d=0.5	d=0.1	d=0.9	d=0.5	d=0.1	d=0.9	d=0.5	d=0.1	d=0.9	d=0.5	d=0.1
f_1	7.14	6.88	5.37	2.96	6.06	6.35	5.03	7.13	7.00	3.95	7.14	7.13	7.09
f_2	7.89	7.81	7.71	7.66	7.77	7.52	7.42	7.86	7.72	5.47	7.89	7.89	7.87
f_3	12.31	12.30	12.24	11.65	12.27	12.01	11.01	11.84	8.99	6.78	12.12	10.64	8.57
f_4	13.02	13.02	13.00	12.76	12.96	12.77	12.49	12.84	12.22	7.54	12.84	12.64	12.61
f_5	18.02	18.01	17.95	15.25	18.01	17.95	16.25	17.12	13.25	8.07	18.01	17.98	17.95
f_6	23.75	23.74	23.62	17.73	23.74	23.65	18.07	22.56	16.98	9.21	23.75	23.72	18.99
f_7	28.44	28.41	27.97	23.30	28.42	28.15	23.50	27.02	20.29	10.43	28.43	28.42	23.07
f_8	32.54	32.49	31.39	28.22	32.50	31.68	28.20	30.93	23.20	11.43	32.54	32.54	23.71
f_9	36.07	36.05	34.39	32.20	36.06	35.16	32.48	34.24	25.56	12.90	36.07	36.07	27.35
f_{10}	41.33	41.05	36.47	36.09	41.10	36.14	35.85	39.5	29.87	13.53	41.33	41.06	28.43
f_{11}	46.97	45.39	42.16	40.44	45.72	42.20	41.19	46.59	35.04	15.69	46.82	41.82	31.96
f_{12}	47.57	47.27	47.22	42.55	47.46	47.40	42.82	46.92	37.20	16.73	47.51	46.86	32.54
f_{13}	49.62	49.57	49.52	47.14	49.37	48.90	47.27	47.53	44.67	20.07	49.60	47.46	36.06
f_{14}	50.85	50.03	50.01	49.49	49.71	49.65	48.75	49.5	46.06	21.92	49.97	49.44	36.83
f_{15}	52.98	52.92	52.71	50.00	52.88	52.62	49.47	50.85	46.67	22.03	52.96	49.78	41.29

Table 2: First 15 frequencies of the 3-stringer composite panel for different damaged components.

The components that were considered damaged are: the upper stringer, case 1; the upper panel, case 3; the central stringer, case 2; and finally the bottom panel, case 4.

Table 2 reports the frequencies obtained from a free-vibration analysis in which the three values of damage, d, were applied for each damage configuration. The diagrams shown in Figure 8 are used to show the variations in the frequencies at each damage level considering the four considered cases. Figure 9 shows the correlation factor, MAC, of the modal shapes for different damage levels.

Figure 8 shows the variations in the frequencies when the upper stringer is considered as the damaged component, that is, for the case 1. The results show that a damage magnitude $d = 0.9$

does not induce a large variation in the frequency values. When a damage level of $d = 0.5$ or $d = 0.1$ is considered, a general reduction of the frequency values appears. Second, third and fourth frequencies seem to be affected slightly by the damage, and this can be explained by looking at the modal shapes in Figure 5. These modes show a notable deformation in the panel area, that is, the damage to the stringer did not produce a strong variation of the response. The correlation between the modal shapes of the undamaged and damaged structures can be observed in Figures 9a, b and c . The MAC value shows that, when a low level of damage ($d = 0.9$) is considered, only the higher modes present variations. Figure 9a shows that the modes 11 and 12 are not closely correlated to those of the intact structure. When the damage level becomes larger, the modes at lower frequencies can also be affected, as shown in Figure 9b, where the 9^{th} mode is clearly not correlated to the modes of the damaged structure. At the maximum damage level, $d = 0.1$, the first modes also show a small correlation value and they may present some switch in the order in which they appear.

Case 2 introduces damage to the central stringer. The frequencies show a similar behavior to those of the previous case, as can be seen in Figure 8. The modes at higher frequencies are affected more for low values of damage, as shown in Figures 9d and 9e, while, for a high damage level, the first modes also show a poor correlation to the undamaged structure, Figure 9f.

The last two cases introduce damage to the two panels. In these cases, the damage has a great influence on the frequency values because it changes the shell-like modes of the panel, as shown in Figure8. A low damage level in the upper panel may produce a strong variation in the higher frequencies, as shown in Figure 9g. An increase in the damage of this component produces a drop in the frequency values and their modal shapes completely lose the correlation with respect to the undamaged structure, as shown in Figures 9h and 9i.

The consequences of damage in the lower panel are not as severe as in the previous case, Figures 9j and 9k, but when a high level of deterioration is considered, Figure 9l, several modes of the damaged structure lose their correspondence with those of the intact structure.

3.3.2. Failure at the layer level

Figures 10a,b and c show the cases in which a single layer fails. In this case, refined models that are able to provide a layer-wise description are mandatory to describe the damage accurately. Table 3 shows the first 15 frequencies considering the three damage levels for each considered case. As in the previous cases, the variations in the frequencies have been reported using the histograms shown in Figure 11.

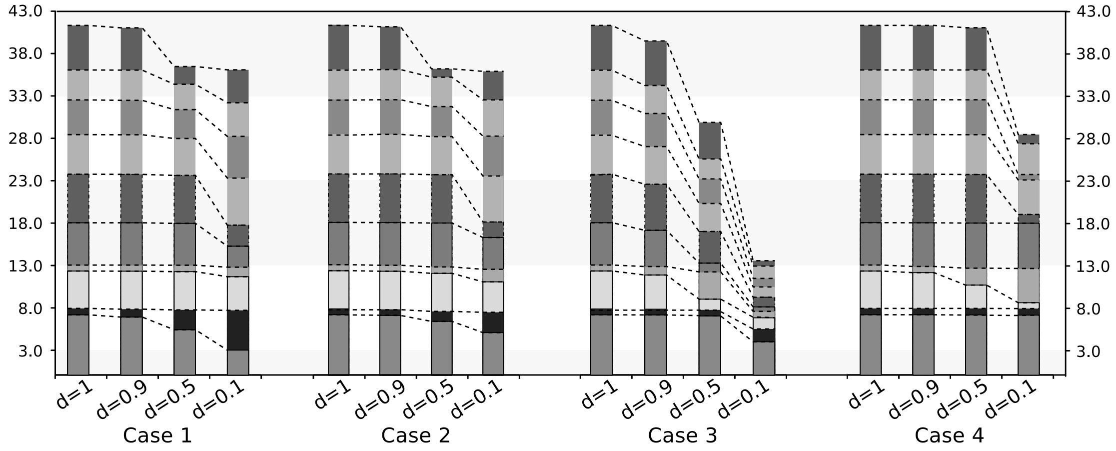

Figure 8: Frequency variations due to different damage conditions.

Cases 5a and 5b consider the failure of an external and an internal layer, respectively. The results reported in Figure 11 show that the failure of the external layer, case 5a, is more critical and produces a larger variation in the natural frequencies. The analysis of the MAC correlation, reported in Figure 12, points our that a reduction of 50% of the external panel integrity, Figure 12b, can have a remarkable effect on the higher modes, while 90% of failure, Figure 12c, completely changes the dynamic response of the structure. When an internal layer fails, more damage is required to change the modal shapes; in fact only when the properties of the panel are reduced by 90%, Figure 12e, is the correlation poor for higher modes. In both cases the first two modes and frequencies are not affected by the damage because they are governed by the stiffness of the stiffeners.

The third case considers the failure of the two external layers. Considering a damage level of $d = 0.9$, the frequencies are reduced slightly, but the higher modal shapes show some variations, as can be seen in the correlation reported in Figure 12g. The increase in the damage causes a drop in the frequency values and the modal correlation only shows values close to unity for few modes. When 90% of the layer properties have been lost, see Figure 12i, only the first mode can be compared with that of the intact structure.

3.3.3. Local damage

In this section, the damage has been considered localized in a small area of the upper panel of the structure. Figure 14a shows the 45 areas where the failure has been considered. A damage value of $d = 0.1$ was applied to all of the four layers of the considered area. Figure 13 shows the variations in the first eight natural frequencies when the failure appears in one of the

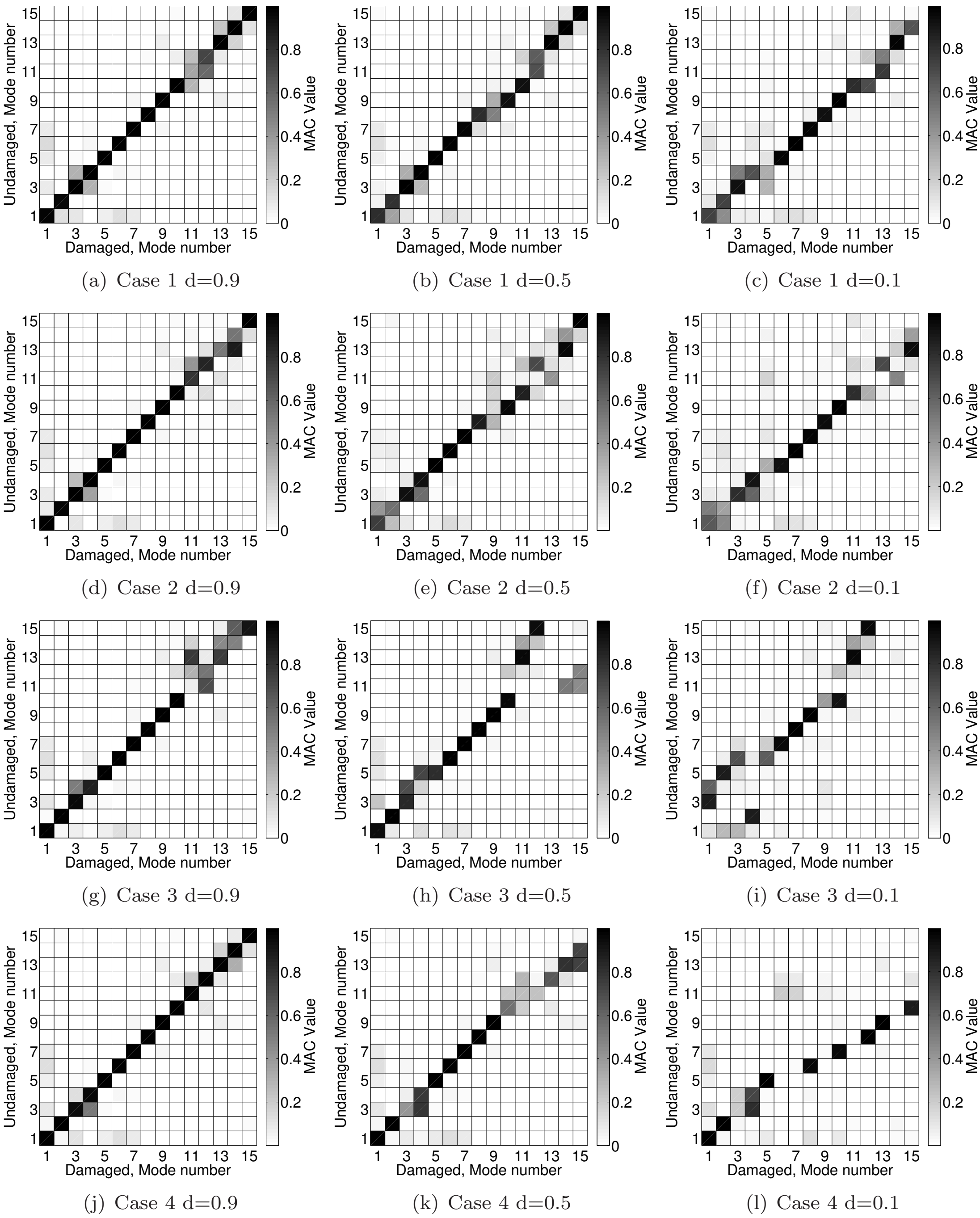

(a) Case 1 d=0.9 (b) Case 1 d=0.5 (c) Case 1 d=0.1

(d) Case 2 d=0.9 (e) Case 2 d=0.5 (f) Case 2 d=0.1

(g) Case 3 d=0.9 (h) Case 3 d=0.5 (i) Case 3 d=0.1

(j) Case 4 d=0.9 (k) Case 4 d=0.5 (l) Case 4 d=0.1

Figure 9: Correlation between the intact and the damaged structures.

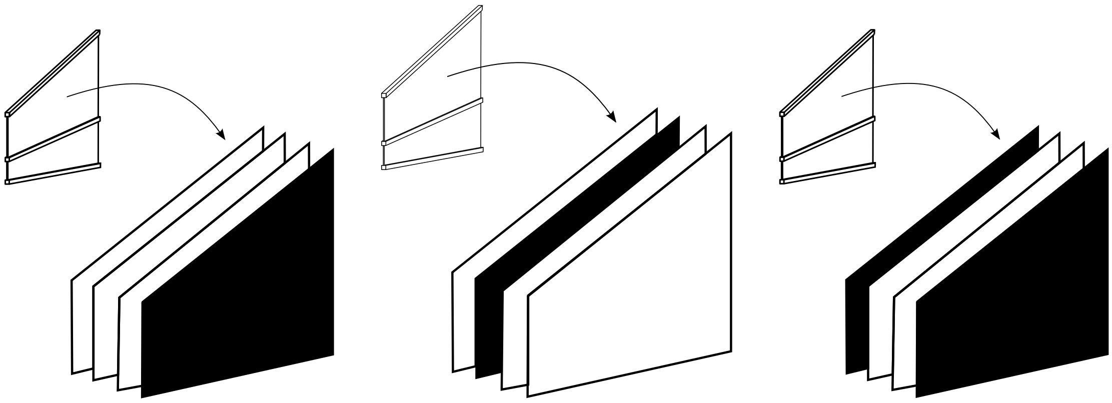

(a) Case 5a (b) Case 5b (c) Case 6

Figure 10: Damaged component cases.

	Undamaged		Case 5a			Case 5b			Case 6	
	d=0	d=0.9	d=0.5	d=0.1	d=0.9	d=0.5	d=0.1	d=0.9	d=0.5	d=0.1
f_1	7.14	7.14	7.12	7.09	7.14	7.13	7.10	7.14	7.09	6.93
f_2	7.89	7.88	7.84	7.79	7.88	7.85	7.80	7.87	7.79	7.70
f_3	12.31	12.17	11.29	9.83	12.24	11.85	11.15	12.01	10.22	7.73
f_4	13.02	12.94	12.75	12.51	12.98	12.85	12.75	12.88	12.61	10.16
f_5	18.02	17.69	16.10	13.66	17.89	17.28	16.34	17.37	14.50	12.37
f_6	23.75	23.32	21.15	17.49	23.59	22.77	21.47	22.89	18.92	13.33
f_7	28.44	27.93	25.51	21.57	28.23	27.23	25.75	27.44	22.96	16.14
f_8	32.54	32.02	29.58	24.99	32.26	30.87	28.73	31.50	26.77	18.90
f_9	36.07	35.29	31.34	26.28	35.92	35.20	34.16	34.54	27.67	20.67
f_{10}	41.33	40.71	37.56	31.17	41.06	39.66	37.40	40.09	33.95	21.84
f_{11}	46.97	46.92	42.31	32.79	46.95	46.85	46.06	46.77	36.89	25.37
f_{12}	47.57	47.33	45.87	39.48	47.49	47.11	46.73	47.74	41.74	27.60
f_{13}	49.62	48.59	46.83	41.45	49.48	48.75	47.54	47.02	46.65	30.30
f_{14}	50.85	49.87	48.16	46.65	49.99	49.76	48.74	49.70	47.21	35.21
f_{15}	52.98	52.14	50.19	46.67	52.64	51.08	50.05	51.39	49.75	35.67

Table 3: First 15 frequencies of the 3-stringer composite panel considering different failure cases at the layer level.

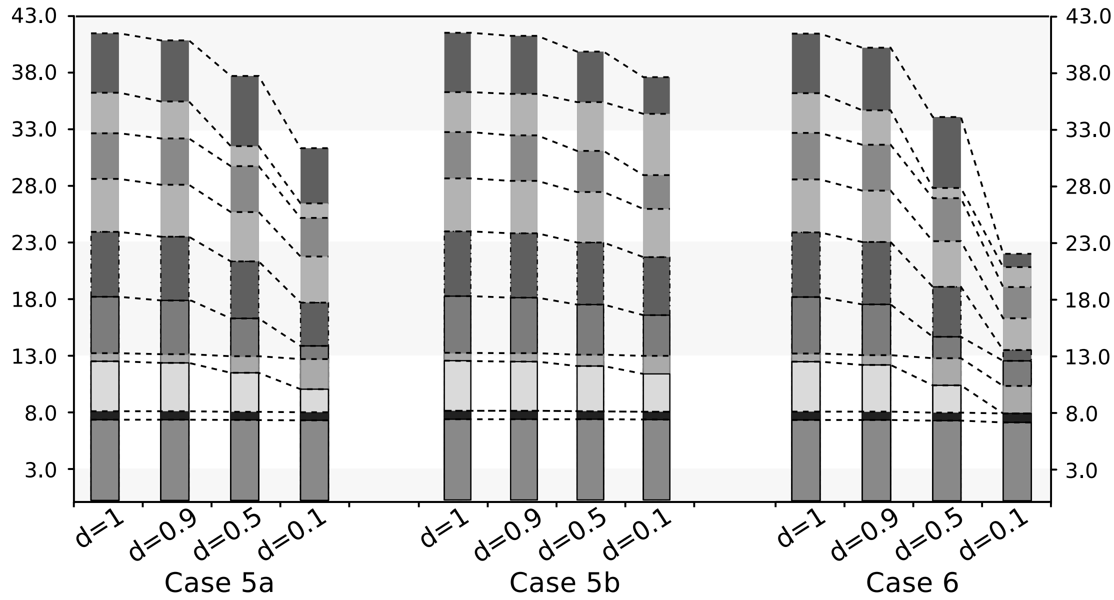

Figure 11: Frequency variation for different failure cases at the layer level.

45 considered areas. This histogram shows that local damage to the panel has only a limited influence on the first frequencies, but can affect the frequencies at higher values. The results highlight which areas of the panel are more sensitive to failure, e.g., failure in panels 11, 12 or 13 has a greater impact on the eighth frequency that failure in area 6; on the other hand failure in panel 27 mainly involves the sixth frequency.

These results can be used to detect the position of damage from variations in the natural frequencies. The results have been elaborated in the colored maps reported in Figure 14. A map has been introduced for each natural frequency, in which the colors represent the variations in frequency values when failure is applied in that area. The darker the color is, the stronger the variation in the frequency value. The parameter, f^*, is reported in Equation 24.

$$f^* = \frac{f}{(f_d - f)_{max}} \left(\frac{f_d - f}{f} \right) \quad \begin{cases} f_d = damaged \quad frequency \\ f = undamaged \quad frequency \end{cases} \tag{24}$$

A value equal to 1 (black color) denotes the area that produces the maximum decrease in frequency.

These maps can be used to locate damage from variations in the natural frequencies. If a drop in the first frequency appears, it is possible to presume that the failure is locate in area 9, as shown in Figure 14b. According to the same approach, a variation in the third frequency

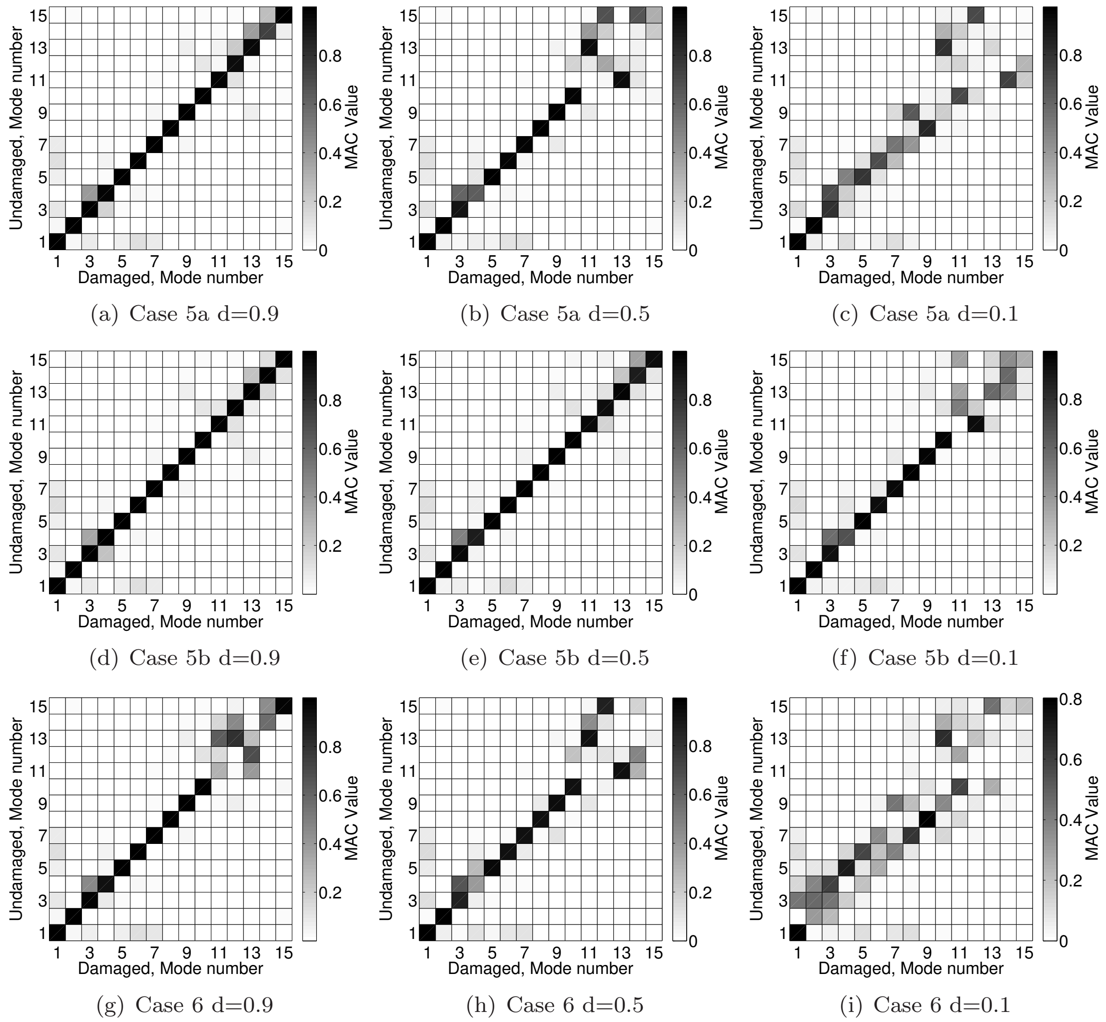

(a) Case 5a d=0.9 (b) Case 5a d=0.5 (c) Case 5a d=0.1

(d) Case 5b d=0.9 (e) Case 5b d=0.5 (f) Case 5b d=0.1

(g) Case 6 d=0.9 (h) Case 6 d=0.5 (i) Case 6 d=0.1

Figure 12: Correlation between the structures with intact and damaged panel layers.

suggests damage in area 21 or 22, see Figure 14d, while a reduction in the fifth frequency denotes failure in area 25.

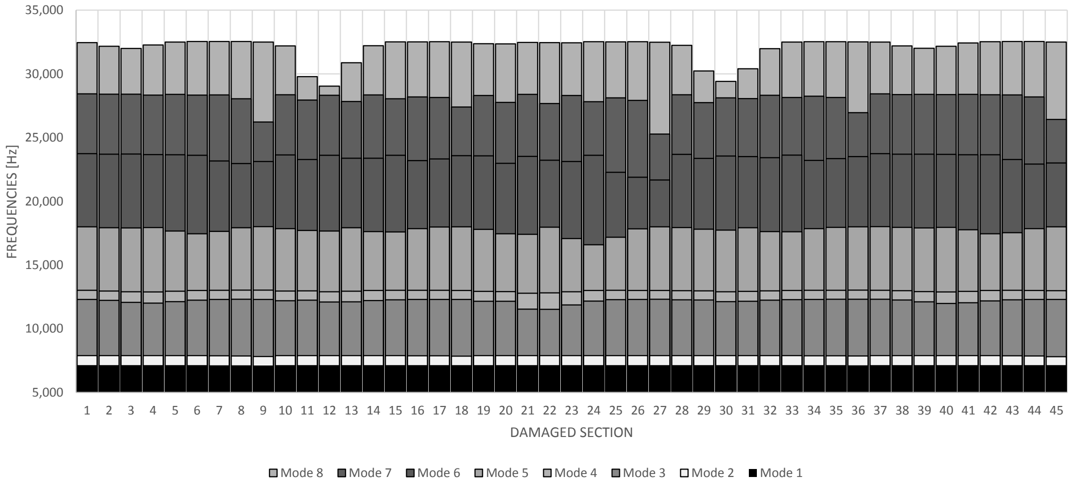

Figure 13: Variations in the first 8 frequencies for different local failures.

3.4. Wing-box structure

An example of a complex aeronautic structure is considered in this section. A multi-component tapered wing-box has been analyzed, Figure 15 shows its geometry. The wing has a length of $L = 5$ m. The tapered shape modifies the chord which changes from a value of $R_1 = 1.48$ m to a value of $R_2 = 0.782$ m. The wing-box thickness is constant, and it is equal to $H = 0.208$ m. The spar is composed of two spar caps and a spar web with a thickness of $t_w = 3$ mm. The spar caps have dimensions equal to $a = 8$ mm, $b = 5$ mm, $c = 20$ mm and $d = 45$ mm. The spars are made of aluminum alloy which has the same proprieties as the previously mentioned material. The skin is a 4-layer laminate made of CFRP, and it has a thickness of $t_s = 4$ mm. The mechanical proprieties of the CFRP are equal to those used in the previous case. There are three ribs made of aluminum, which are placed at $Yr = 1,6666667$ m. Their thickness is equal to t_s. The central spar is aligned with the Y_G-axis.

For the sake of brevity, only the effects of six different failures have been considered for the first bending and first torsional modes. A solid Nastran solid model, with more than 400000 DOFs, was used for validation purposes. The LE model used six 4-node beam elements, along the length of the spar-caps and one 3-node beam element placed over the thickness to describe each web and each layer of the skin. The same layout was used for the ribs. Figure 16 shows

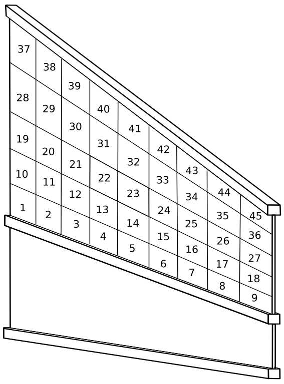

(a) Damaged area numbering

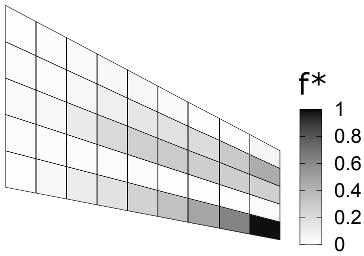

(b) Frequency 1

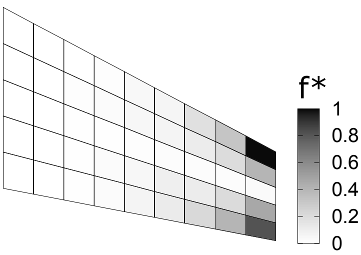

(c) Frequency 2

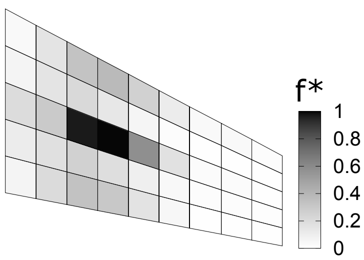

(d) Frequency 3

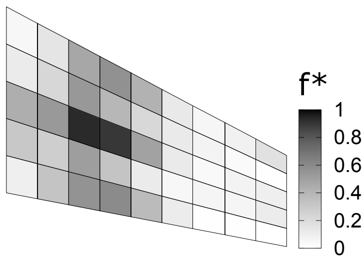

(e) Frequency 4

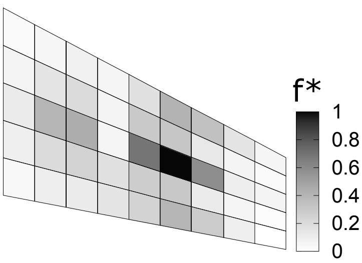

(f) Frequency 5

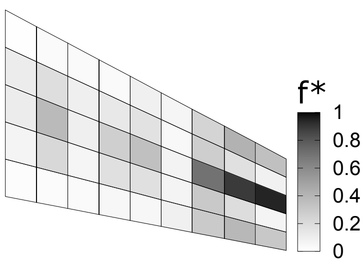

(g) Frequency 6

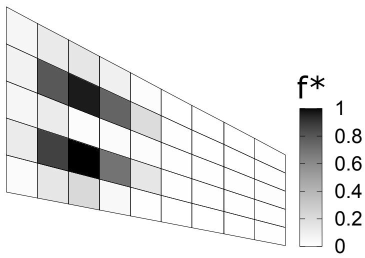

(h) Frequency 8

Figure 14: Damage influence maps. For each frequency the map shows the area which, if damaged, has the greatest effect on that frequency value.

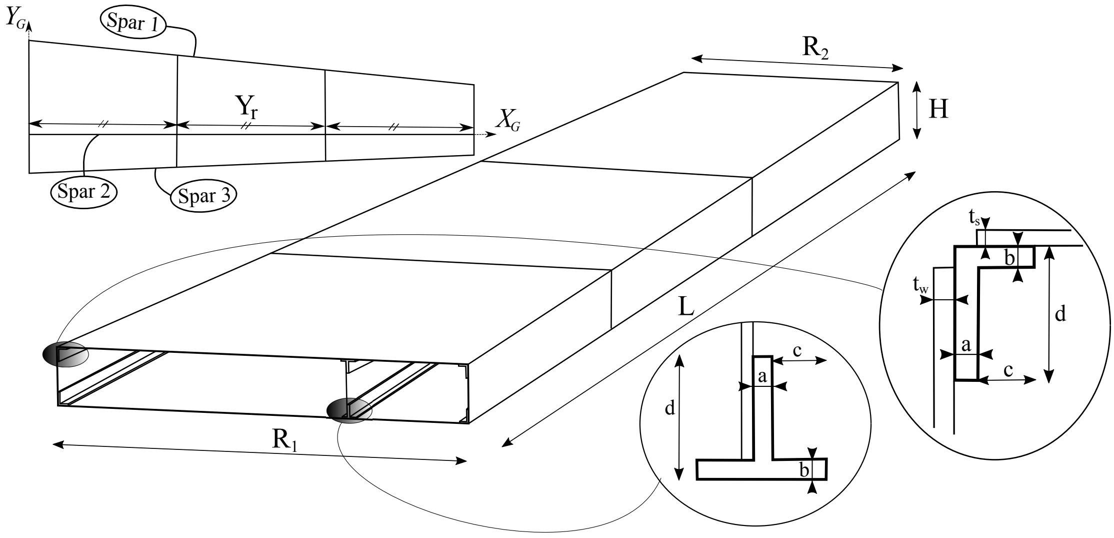

Figure 15: Considered wing structure.

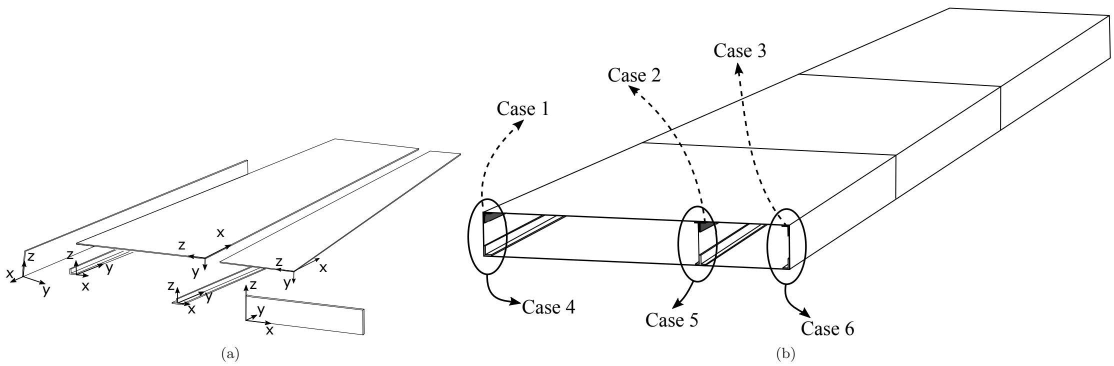

Figure 16: Local beam frames (a) and Damage cases (b)

	Solid	LE Model
DOFs	>400000	42468
1^{st} B	9.57	9.58
1^{st} T	38.54	39.40

Table 4: Assessment of the present model. First bending mode, 1^{st} B. First torsional mode, 1^{st} T.

		Top Spar Caps failure			Complete Spar failure		
	Undamaged	Case 1	Case 2	Case 3	Case 4	Case 5	Case 6
1^{st} B	9.58	9.35	9.3 0	9.35	8.96	8.87	9.01
1^{st} T	39.40	38.91	39.15	39.18	35.70	37.73	37.67

Table 5: Different Conditions of damaged spars with a damage level of $d = 0.1$.

the orientation of the local frame for each component, where y identifies the beam axis. The model has 42468 DOFs. Table 4 shows the results obtained using the present model and the solid model built using the commercial Nastran code. The results show the accuracy of the present model, even when complex structures are considered. Moreover, the LE Model provides accurate results, but only uses a fraction of the DOFs required by the Solid model which, in order to respect the geometrical aspect ratio limitation, requires a huge number of elements for the analysis of thin-walled structures.

The first three damaged configurations, cases 1 to 3, only consider the failure of the top caps of each spar. Cases 4 to 6 consider the complete failure of the spar, that is, both the caps and web were considered damaged. All six cases consider a damage parameter, d, equal to 0.1.

Table 5 shows the frequencies obtained from the analyses of the six configurations. The first bending frequency is almost unaffected by the failure of the caps but it show a decrease when the frontal and the central spars are damaged. The failure of the central spar, case 5, produces a drop in the first bending frequency of 7.4%.

An analysis of the modal shapes shows more details about the effects of the failure. Figure 17*a* presents the modal shapes of the first bending mode, considering the tip section of the wing. The damage located in the caps of the first spar reduces the torsional effect due to the tapered shape. On the other hand, case 3 increases this effect. The effects of the damage on the whole spar are more significant, as shown in Figure 17*b*. In this case, it can be observed that the failure of the first spar changes the torsion angle. This could be of great interest when coupling phenomena are present, e.g., in aero-elastic phenomena.

As expected, when the first torsional mode is considered, the critical component is the first

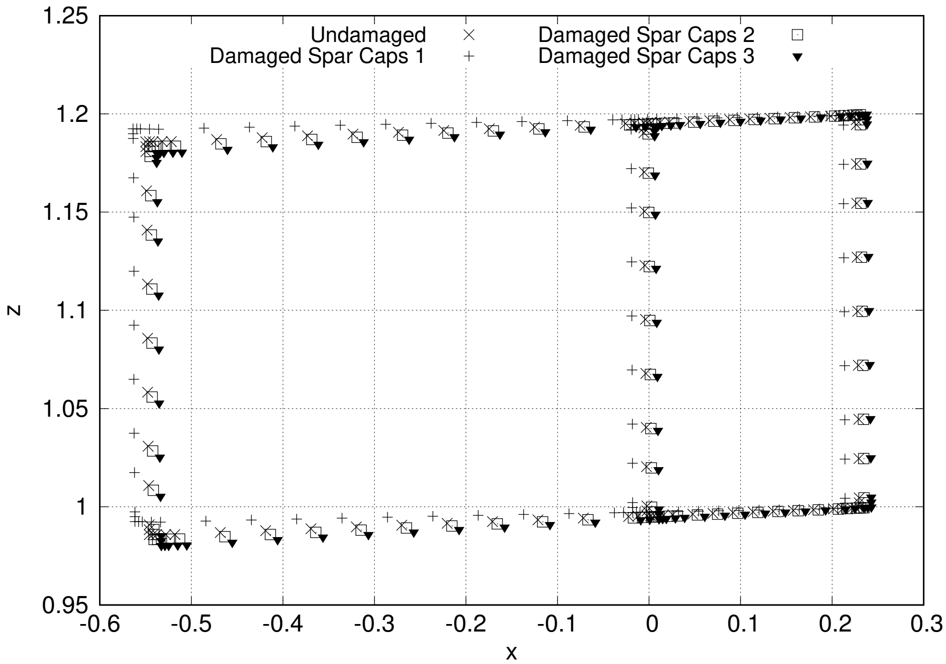

(a) Failure of the spar cap

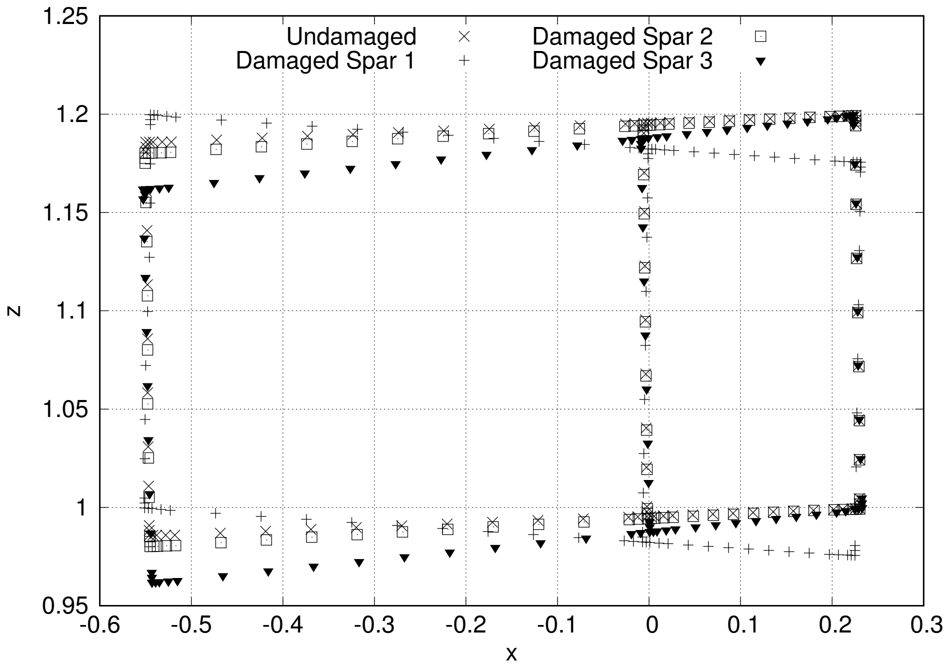

(b) Failure of the whole spar

Figure 17: Influence of damage on the 1^{st} bending mode.

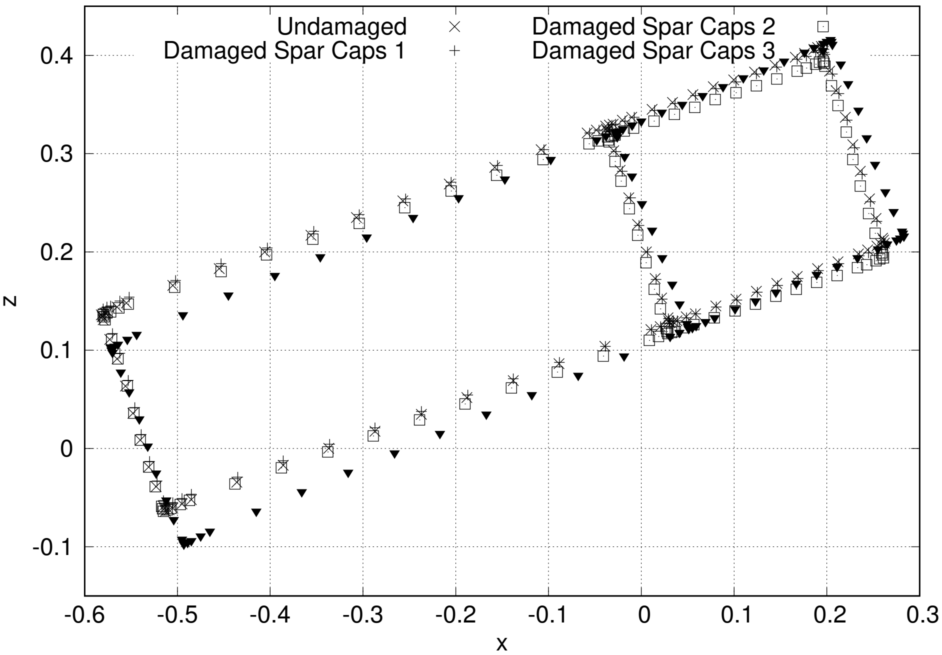

(a) Failure of the spar cap

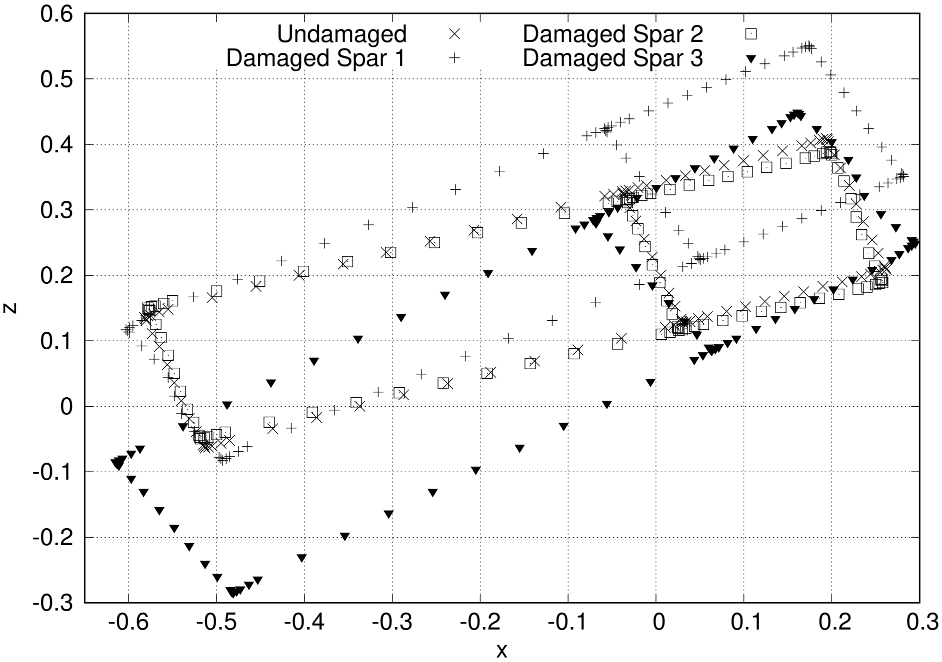

(b) Failure of the whole spar

Figure 18: Influence of damage on the 1^{st} torsional mode.

spar. The failure of this element produces a strong reduction in the torsional stiffness, because of the reduction in the strength of the frontal closed cell. The Case 4 failure introduces a decrease of 9.4% in the frequency value. Figure 18 shows the effects on the modal shape at the tip of the wing. The damage of the whole spar introduces sensible effects, particularly for case 4 and case 6.

4. Final Remarks

In this work, the capabilities of an advanced one-dimension model have been exploited to study the dynamic response of damaged composite structures. This model introduces a three-dimensional description of the structure with no geometrical approximations and a deformable cross-section of the beam. These features allow a quasi-3D solution to be obtained and make the models able to deal with non-classical and local effects due to global and local failure of a complex composite structure. The failure of the structure has been considered by introducing degradation of the material properties, thus the stiffness in the damaged area is reduced. The present model has been used to study the variations in the natural frequencies of a structure that has suffered from the failure of a single component, the failure of one or more layers or the failure of a small area of a panel. The Modal Assurance Criteria, MAC, has been used to evaluate the variations in the modal shapes. The following remarks can be made concerning the results:

- In all the considered cases the present model has been able to accurately predict the natural frequencies and the modal shapes, with a reduction in the computational costs, compared with solid models.
- The component-wise approach allows the failure of a single component to be introduced.
- The layer-wise model used in the present work makes it possible to consider the damage of each single layer, and thus to evaluate the consequences on the natural frequencies and modal shapes.
- The analysis of a local failure and the derivation o a database of possible scenarios could lead to the fast detection of failure on the basis of variations in the natural frequency.
- The present approach can easily be extended to complex structures, such as wing boxes.

In short, thanks to its efficiency and accuracy, the present model can be used to characterize the behavior of complex structures when they suffer from failure at different levels. The present results could be used to derive future approaches for the health monitoring of composite structures or their maintenance procedure.

References

[1] Z. Zhang, K. Shankar, E. Morozov, M. Tahtali, Vibration-based delamination detection in composite beams through frequency changes, Journal of Vibration and Control 22 (2) (2016) 496–512. doi:10.1177/1077546314533584.

[2] R. Capozuzza, Vibration of cfrp cantilever beam with damage., Composite Structures 116 (2014) 211–222.

[3] Y. Wang, M. Liang, J. Xiang, Damage detection method for wind turbine blades based on dynamics analysis and mode shape difference curvature information., Mechanical Systems and Signal Processing 48 (2014) 351–367.

[4] K. Nguyen, Mode shapes analysis of a cracked beam and its application for crack detection., Journal of Sound and Vibration 333 (3) (2014) 848–872.

[5] H. Pollayi, W. Yu, Modeling matrix cracking in composite rotor blades within vabs framework., Composite Structures 110 (2014) 62–76. doi:10.1016/j.compstruct.2013.11.012.

[6] M. Perez, L. Gil, M. Sánchez, , S. Oller, Comparative experimental analysis of the effect caused by artificial and real induced damage in composite laminates., Composite Structures 112 (2014) 169–178.

[7] L. Euler, De curvis elasticis. Methodus inveniendi lineas curvas maximi minimive proprietate gaudentes, sive solutio problematis iso-perimetrici lattissimo sensu accepti.

[8] S. Timoshenko, J. Goodier, Theory of elasticity, McGraw-Hill, 1970.

[9] P. Cicala, Sulle travi di altezza variabile, Laboratorio di Aeronautica, Tipografia Vincenzo Bona, Turin, Italy, 1939.

[10] D. Just, Plane frameworks of tapering box and I-section, Journal of the Structural Division 103 (1) (1977) 71–86.

[11] C. Brown, Approximate stiffness matrix for tapered beams, Journal of Structural Engineering 110 (12) (1984) 3050–3055. doi:10.1061/(ASCE)0733-9445(1984)110:12(3050).

[12] H. Schreyer, Elementary theory in linearly tapered beams, Journal of the Engineering Mechanics Division 104 (3) (1978) 515–527.

[13] E. Carrera, A. Pagani, M. Petrolo, Component-wise method applied to vibration of wing structures., Journal of Applied Mechanics 80 (4) (2013) Paper 041012. doi:10.1115/1.4007849.

[14] E. Carrera, A. Pagani, Accurate response of wing structures to free-vibration, load factors, and nonstructural masses., AIAA Journal 54 (1) (2016) 227–241.

[15] E. Zappino, E. Carrera, Multidimensional model for the stress analysis of reinforced shell structure, AIAA JournalIn Press. doi:10.2514/1.J056384.

[16] E. Carrera, E. Zappino, T. Cavallo, Accurate free vibration analysis of launcher structures using refined 1d models, International Journal of Aeronautical and Space Sciences 16 (2) (2015) 206–222. doi:10.5139/IJASS.2015.16.2.206.

[17] E. Carrera, A. Pagani, M. Petrolo, Free vibrations of damaged aircraft structuresby component-wise analysis., AIAA JOURNAL 54 (10) (2016) 3091–3106. doi:10.2514/1.J054640.

[18] R. Allemang, D. Brown, A correlation coefficient for modal vector analysis., Proceedings of the International Modal Analysis Conference (1982) 110–116.

[19] O. Salawu, C. Williams, Bridge assessment using forcedvibration testing., Journal of Structural Engineering 121 (2) (1995) 161–173.

[20] E. Zappino, A. Viglietti, E. Carrera, The analysis of tapered structures using a component-wise approach based on refined one-dimensional models., Aerospace Science and Technology 65 (2017) 141–156.

[21] E. Zappino, A. Viglietti, E. Carrera, Analysis of tapered composite structures using a refined beam theory., Composite Structures 183 (2017) 42–52.

[22] E. Carrera, C. M., M. Petrolo, E. Zappino, Finite Element Analysis of Structures Through Unified Formulation, John Wiley & Sons, 2014.

[23] S. Tsai, Composites Design, 4th Edition, Dayton, Think Composites, 1988.

[24] J. Reddy, Mechanics of laminated composite plates and shells. Theory and Analysis, 2nd Edition, CRC Press, 2004.

[25] E. Carrera, G. Giunta, M. Petrolo, Beam Structures: Classical and Advanced Theories, Wiley, Hoboken, 2011.

[26] E. Carrera, A. Pagani, M. Petrolo, Classical, refined, and component-wise analysis of reinforced-shell wing structures., AIAA JOURNAL 51 (5) (2013) 1255–1268.

[27] E. Carrera, M. Petrolo, Refined Beam Elements With Only Displacement Variables and Plate/Shell Capabilities., Meccanica 47 (3) (2012) 537–556.

[28] E. Carrera, E. Zappino, Carrera Unified Formulation for Free-Vibration Analysis of Aircraft Structures., AIAA Journal 1 (54) (2016) 280–292.

[29] T. Cavallo, E. Zappino, E. Carrera, Component-wise vibration analysis of stiffened plates accounting for stiffener modes., CEAS Aeronautical Journal 8 (2) (2017) 385–412.